to the pool RNA was determined by the gel mobility of 3′-terminal fragments cleaved by a DNA enzyme[28] targeted to the 3′ constant segment. RNAs extended with ^{4S}U (for use as synthetic standards) were generated, using App^{4S}U instead of AppRpp.

Ribozyme selection. ^{4S}Ura was synthesized[29] and further purified by reverse-phase HPLC. For each round of selection the RNA-pRpp pool was incubated with ^{4S}Ura (Fig. 2b) using the concentrations and incubation times outlined in Fig. 3 (≤0.3 μM pool RNA, 50 mM Tris-HCl pH 7.5, 150 mM KCl, 25 mM $MgCl_2$, 1 mM $CaCl_2$, 0.5 mM $MnCl_2$ at 23 °C). Ribozyme reactions were stopped by the addition of one volume of gel loading buffer (90% formamide, 50 mM EDTA). RNA with a 3′-terminal ^{4S}U was resolved from other species on denaturing APM gels[14,30] (8 M urea/5% polyacrylamide gels, cast with 80 μM *N*-acryloylaminophenylmercuric acetate). During each round of selection, the ribozyme reaction was split in half. One half contained radiolabelled pool RNA that facilitated the detection and purification of emergent ribozymes; the other half contained unlabelled pool and a trace amount of radiolabelled synthetic standard (an RNA pool with a 3′-terminal ^{4S}U but with primer-binding sequences incompatible with reverse transcription and PCR) that was used to locate and monitor the recovery of reacted RNA. The gel fragment containing RNA-^{4S}U was excised (Fig. 2c), and RNA was eluted in 300 mM NaCl, 20 mM DTT, then precipitated with ethanol. After round 1, RNA containing ^{4S}U was further purified on a second mercury gel and then biotinylated (Fig. 2d) by resuspending precipitated RNA in 25 mM potassium phosphate pH 8.4, 3 mM iodoacetyl-LC-biotin (Pierce), 50% v/v dimethylformamide. After 3 h at room temperature in the dark, the reaction was quenched with DTT and diluted 10-fold; RNA was then twice precipitated with ethanol to remove excess biotin. About 75% of material end-labelled with ^{4S}U was biotinylated, as judged by a streptavidin gel-shift assay. Capture of biotinylated RNA, reverse transcription, PCR amplification and transcription *in vitro* were as described previously[25].

Ribozyme assays. Unless stated otherwise, ribozyme isolates were assayed under conditions similar to those of the selection (0.5 μM ^{32}P-labelled ribozyme RNA, 50 mM *N*,*N*-(bis-2-hydroxyethyl)-2-aminoethanesulphonic acid (BES) pH 7.5, 150 mM KCl, 25 mM $MgCl_2$, 0.5 mM $MnCl_2$ at 23 °C). The rate of ^{4S}U synthesis (k_{obs}) at a given ^{4S}Ura concentration was determined by the best fit of k and β to the equation $F = \beta(1 - e^{-kt})$, where F is the fraction reacted (ascertained by phosphorimaging of the APM gel), $k = k_{obs} + k_{hyd}$, $\beta = F_{max}k_{obs}/(k_{obs} + k_{hyd})$, k_{hyd} is the rate of pRpp hydrolysis, and t is time. F_{max}, the maximal active fraction (typically 0.15–0.20) was determined by using time courses with ^{4S}Ura in excess of 4 mM. Factors contributing to the low F_{max} values included: incomplete pRpp ligation (lowering F_{max} by 10–30%), 3′ heterogeneity from untemplated residues added during transcription (lowering F_{max} by 40–50%), and ribozyme misfolding. The k_{hyd} values were determined by varying ^{4S}Ura concentration and observing differences in the asymptotic fraction reacted. The k_{hyd} values were confirmed independently by monitoring the inactivation of RNA-pRpp in the absence of ^{4S}Ura. The rate of uridine synthesis was determined by using isolate a15 and a random-sequence control RNA, both activated with pRpp. Each RNA (7 μM) was incubated with 0.5 mCi [5,6-^{3}H]uracil (NEN) in standard buffer conditions. At 0, 2, 4 and 8 h, 160 μl aliquots were quenched by the addition of EDTA and unlabelled uracil. RNA was filtered (Centricon spin filters; Amicon), purified on a polyacrylamide gel and precipitated with ethanol. Uracil counts associated with the RNA were determined by scintillation (Formula-989 fluid, Packard) and corrected for RNA recovery. A similar approach with [2-^{14}C]uracil indicated a comparable rate (within twofold). Additional analysis of RNA recovered from the scintillation fluid (precipitation with NaCl and six volumes of ethanol, and resuspension with unlabelled uridine) confirmed that the incorporated counts were from 3′-terminal uridine synthesis; RNA was base-hydrolysed and nucleotides were separated by reverse-phase HPLC and scintillation-counted. The uncatalysed reaction rates were examined with a 9-nt RNA-pRpp conjugate that was ^{32}P-labelled at its 5′ terminus. After incubation with 6.4 mM ^{4S}Ura for 4 days in the buffer used for the selection, no RNA-p^{4S}U product was observed on APM gels. A single gel would have readily detected uncatalysed RNA-p^{4S}U formation with a rate $\geq 2 \times 10^{-6}$ M^{-1} min^{-1} (correcting for the RNA-pRpp lost to hydrolysis), whereas a serial APM gel analysis lowered detection limits to 6×10^{-7} M^{-1} min^{-1}. The RNA-pRpp hydrolysed during the 4-day time course indicated an uncatalysed k_{hyd} of 9×10^{-5} min^{-1}.

Received 13 March; accepted 20 July 1998.

1. Joyce, G. F. & Orgel, L. E. in *The RNA World* (eds Gesteland, R. F. & Atkins, J. F.) 1–25 (Cold Spring Harbor Lab., Cold Spring Harbor, NY, 1993).
2. Fuller, W. D., Sanchez, R. A. & Orgel, L. E. Studies in prebiotic synthesis VI. Synthesis of purine nucleosides. *J. Mol. Biol.* **67,** 25–33 (1972).
3. Fuller, W. D., Sanchez, R. A. & Orgel, L. E. Studies in prebiotic synthesis VII. Solid-state synthesis of purine nucleosides. *J. Mol. Evol.* **1,** 249–257 (1972).
4. Larralde, R., Robertson, M. P. & Miller, S. L. Rates of decomposition of ribose and other sugars: implications for chemical evoution. *Proc. Natl Acad. Sci. USA* **92,** 8158–8160 (1995).
5. Mizuno, T. & Weiss, A. H. Synthesis and utilization of formose sugars. *Adv. Carbohyd. Chem. Biochem.* **29,** 173–227 (1974).
6. Pitsch, S., Eschenmoser, A., Gedulin, B., Hui, S. & Arrhenius, G. Mineral induced formation of sugar phosphates. *Origin Life Evol. Biosphere* **25,** 297–334 (1995).
7. Oro, J. Mechanism of synthesis of adenine from hdyrogen cyanide under possible primitive earth conditions. *Nature* **191,** 1193–1194 (1961).
8. Sanchez, R. A., Ferris, J. P. & Orgel, L. E. Studies in prebiotic synthesis. II. Synthesis of purine precursors and amino acids from aqueous hydrogen cyanide. *J. Mol. Biol.* **30,** 223–253 (1967).
9. Ferris, J. P., Sanchez, R. A. & Orgel, L. E. Studies in prebiotic synthesis. 3. Synthesis of pyrimidines from cyanoacetylene and cyanate. *J. Mol. Biol.* **33,** 693–704 (1968).
10. Stoks, P. G. & Schwartz, A. W. Uracil in carbonaceous meteorites. *Nature* **282,** 709–710 (1979).
11. Robertson, M. P. & Miller, S. L. An efficient prebiotic synthesis of cytosine and uracil. *Nature* **375,** 772–774 (1995).
12. Bhatia, M. B., Vinitsky, A. & Grubmeyer, C. Kinetic mechanism of orotate phosphoribosyltransferase from *Salmonella typhimurium*. *Biochemistry* **29,** 10480–10487 (1990).
13. Tao, W., Grubmeyer, C. & Blanchard, J. S. Transition state structure of *Salmonella typhimurium* orotate phosphoribosyltransferase. *Biochemistry* **35,** 14–21 (1996).
14. Igloi, G. L. Interaction of tRNAs and of phosphorothioate-substituted nucleic acids with an organomercurial. Probing the chemical environment of thiolated residues by affinity electrophoresis. *Biochemistry* **27,** 3842–3849 (1988).
15. Wierzchowski, K. L., Litonska, E. & Shugar, D. Infrared and ultraviolet studies on the tautomeric equilibria in aqueous medium between monoanionic species of uracil, thymine, 5-fluorouracil, and other 2,4-diketopyrimidines. *J. Am. Chem. Soc.* **87,** 4621–4629 (1965).
16. Psoda, A., Kazimierczuk, Z. & Shugar, D. Structure and tautomerism of the neutral and monoanionic forms of 4-thiouracil derivatives. *J. Am. Chem. Soc.* **96,** 6832–6839 (1974).
17. Bartel, D. P. & Szostak, J. W. Isolation of new ribozymes from a large pool of random sequences. *Science* **261,** 1411–1418 (1993).
18. Gray, M. W. The presence of 2′-O-methylpseudouridine in the 18S + 26S ribosomal ribonucleates of wheat embryo. *Biochemistry* **13,** 5453–5463 (1974).
19. Jaffe, E. K. & Cohn, M. Diastereomers of the nucleoside phosphorothioates as probes of the structure of the metal nucleotide substrates and of the nucleotide binding site of yeast hexokinase. *J. Biol. Chem.* **254,** 10839–10845 (1979).
20. Benner, S. A., Ellington, A. D. & Tauer, A. Modern metabolism as a palimpsest of the RNA world. *Proc. Natl Acad. Sci. USA* **86,** 7054–7058 (1989).
21. Michel, F., Hanna, M., Green, R., Bartel, D. P. & Szostak, J. W. The guanosine binding site of the *Tetrahymena* ribozyme. *Nature* **342,** 391–395 (1989).
22. Been, M. D. & Perrotta, A. T. Group I intron self-splicing with adenosine: evidence for a single nucleoside-binding site. *Science* **252,** 434–437 (1991).
23. Gold, L., Polisky, B., Uhlenbeck, O. & Yarus, M. Diversity of oligonucleotide functions. *Annu. Rev. Biochem.* **64,** 763–797 (1995).
24. Ekland, E. H. & Bartel, D. P. RNA-catalysed RNA polymerization using nucleoside triphosphates. *Nature* **382,** 373–376 (1996).
25. Ekland, E. H. & Bartel, D. P. The secondary structure and sequence optimization of an RNA ligase ribozyme. *Nucleic Acids Res.* **23,** 3231–3238 (1995).
26. England, T. E., Gumport, R. I. & Uhlenbeck, O. C. Dinucleoside pyrophosphates are substrates for T4-induced RNA ligase. *Proc. Natl Acad. Sci. USA* **74,** 4839–4842 (1977).
27. Lohrmann, R. & Orgel, L. E. Preferential formation of (2′-5′)-linked internucleotide bonds in non-enzymatic reactions. *Tetrahedron* **34,** 853–855 (1978).
28. Santoro, S. W. & Joyce, G. F. A general purpose RNA-cleaving DNA enzyme. *Proc. Natl Acad. Sci. USA* **94,** 4262–4266 (1997).
29. Mizuno, Y., Ikehara, M. & Watanabe, K. A. Potential antimetabolites. I. Selective thiation of uracil and 1,2,4-triazine-3,5(2*H*,4*H*)-dione (6-azauracil). *Chem. Pharmac. Bull.* **10,** 647–652 (1962).
30. Wecker, M., Smith, D. & Gold, L. *In vitro* selection of a novel catalytic RNA: characterization of a sulfur alkylation reaction and interaction with a small peptide. *RNA* **2,** 982–994 (1996).

Acknowledgements. We thank J. Stubbe, P. Zamore and members of the lab for helpful comments on the manuscript, and G. Joyce for providing the sequence of the RNA-cleaving DNA enzyme[28] before publication. This work was supported by an MRC (Canada) postdoctoral fellowship to P.J.U. and a grant from the Searle Scholars Program/The Chicago Community Trust to D.P.B.

Correspondence and requests for materials should be addressed to D.P.B. The nine active sequences have been deposited in GenBank under accession numbers AF051883–51891.

Deep-ocean gradients in the concentration of dissolved organic carbon

Dennis A. Hansell & Craig A. Carlson

Bermuda Biological Station for Research, Inc., St Georges, GE01, Bermuda

There is as much carbon in dissolved organic material in the oceans as there is CO_2 in the atmosphere[1], but the role of dissolved organic carbon (DOC) in the global carbon cycle is poorly understood. DOC in the deep ocean has long been considered to be uniformly distributed[2,3] and hence largely refractory to biological

Table 1 Deep ocean concentrations of dissolved organic carbon

Location	Position	Depth range (m)	DOC (μM)	*N*	s.d.	Comments
North Atlantic	75° N, 0° W	1,250–3,650	48.1	10	0.3	2 vertical profiles, April 1995
	48° N; 13°, 41° and 48° W	1,100–4,800	45.1	19	0.4	Mean of 3 stations, 1997
	32° N, 164° W	1,000–4,000	43.6	35	0.3	Mean of 6 profiles, 1997
Circumpolar Current	60° S, 170° W	1,000–4,000	41.5	7	0.4	Single profile, 1997*
	61° S, 170° W	2,000	41.9	33	0.3	Mean of replicate samples, 1996*
Ross Sea	75–77° S, 178° E–178° W	0–700	41.7	241	0.3	Regional mean, late winter 1996*
Indian Ocean	36° S, 95° E	1,000–2,000	43.3	3	0.1	Single profile, 1995
	32° S, 80° E	1,500–2,000	42.9	2	–	Single profile, 1995
	26° S, 80° E	1,000–2,000	43.3	3	0.0	Single profile, 1995
	14° S, 80° E	1,000–4,000	42.9	6	0.7	Single profile, 1995
	8° S, 80° E	1,500–5,500	43.6	3	0.3	Single profile, 1995
	3° N, 80° E	1,500–3,000	43.3	4	0.2	Single profile, 1995
Arabian Sea	13–20° N, 60–65° E	1,000–4,300	42.8	27	0.8	Mean of 8 stations, 1995*
Pacific Ocean	56.5° S, 170° W	1,000–5,000	42.3	5	0.3	Single profile, 1996
	52.5° S, 170° W	1,000–5,000	42.3	5	0.1	Single profile, 1996
	33.5° S, 170° W	1,000–5,000	43.0	5	0.1	Single profile, 1996
	0° S, 170° W	1,000–5,000	42.7	4	0.1	Single profile, 1996
	22.75° N, 158° W	900–4,750	38.8	9	0.9	Single profile, 1997
	58° N, 148° W	1,000–1,500	33.8	3	0.4	Single profile, 1997

Details on the sampling and results from the deep ocean survey of DOC concentrations. All samples were collected with Niskin bottles on CTD rosettes. DOC is the mean of the concentrations in one or more vertical profiles at a given site; *N* is the number of depths sampled over the depth range indicated; s.d. is the standard deviation of the means from the several depths at each site; the dates indicate the year of sampling. Samples from the South Atlantic Ocean remain lacking in this survey. Samples selected for calculation of the mean were those from the zone in the water column (generally >1,000 m) where vertical gradients in DOC concentration were not evident. Bottom depth in the Ross Sea is generally <1,000 m, so shallower depths were taken as no vertical gradient was evident.

*These analyses were performed at sea. All other analyses were done over a period of a few months in the shore-based laboratory. Samples not run at sea were stored at –20 °C in precleaned glass vials or polyethylene bottles. These storage techniques have been thoroughly tested over the past several years and have demonstrated no artefactual results on the micromolar scale. Deep Sargasso Sea reference water (2,600 m; DOC, 43.6 ± 0.2 μM) was acidified with H_3PO_4, ampoulated in glass and stored unfrozen. Experience with this reference material has shown that it remains stable for a minimum of several years. While in the field, deep Sargasso Sea reference water was evaluated every fourth to sixth analysis. While in the shore laboratory, the reference material was run every second and third analysis. High-precision analyses for DOC concentrations were done using a non-commercial high-temperature combustion system with procedures and blank corrections as described[29]. Analytical precision in this work on replicated samples was approximately 0.3 μM. Samples were not filtered, but because particulate organic carbon loads (organic carbon retained on a GF/F filter) are generally less than a few tenths of micromolar in the deep ocean, the data are reported as DOC.

decay[4]. But the turnover of DOC, and therefore its contribution to the carbon cycle, has been evident from radiocarbon dating studies[5,6]. Here we report the results of a global survey of deep-ocean DOC concentrations, including the region of deep-water formation in the North Atlantic Ocean, the Circumpolar Current of the Southern Ocean, and the Indian and Pacific oceans. DOC concentrations decreased by 14 micromolar from the northern North Atlantic Ocean to the northern North Pacific Ocean, representing a 29% reduction in concentration. We evaluate the spatial patterns in terms of source/sink processes. Inputs of DOC to the deep ocean are identifiable in the mid-latitudes of the Southern Hemisphere, but the mechanisms have not been identified with certainty.

Deep water samples were collected from numerous sites in the global ocean (Fig. 1, Table 1). Measured concentrations of DOC were determined relative to deep Sargasso Sea reference water (see Table 1 for methods). Concentrations were highest in the Greenland Sea (48 ± 0.3 μM C), decreasing to 45.1 ± 0.4 and 43.6 ± 0.3 μM near 48° N and 32° N, respectively, in the North Atlantic (Fig. 2). Concentrations in the Circumpolar Current (61° S) and the Ross Sea (75° S) were 41.5–41.9 μM, then increased to the north in the central Indian Ocean and Arabian Sea (42.8–43.6 μM C), as well as in the western South Pacific Ocean (42.3–43.0 μM C). Concentrations decreased into the North Pacific, where the global low of 33.8 ± 0.4 μM was found at the northernmost site sampled. Previously published data sets were not used in our synthesis because a reference material common to that used here was not employed.

DOC in the deep ocean comprises a large fraction of very old material (6,000 yr) and a smaller fraction of young material[5,6]. The changes seen in DOC concentration along the deep path of the global 'conveyor belt'[7] result from: the addition of young material at the sites of deep-water formation (particularly in the North Atlantic) and its microbial consumption at depth; isopycnal and diapycnal mixing of waters with various DOC loads; and small additions (solubilization)[8] and losses (adsorption)[9] as a result of transformation of particulate matter. That the large gradient seen in Fig. 1 was created by seasonal variability in deep DOC, perhaps linked to seasonality in the vertical flux of biogenic particles, is discounted by the lack of short-term variability in the deep Sargasso and Arabian seas (Table 2). These two sites show strong seasonality in vertical particle flux, with flux being particularly high in the spring in the Sargasso Sea[10] and in late summer in the Arabian Sea[11], but little variability in deep DOC over those periods.

The Greenland Sea samples are our best representation for concentrations of DOC in the source water for North Atlantic Deep Water (NADW) formation. NADW overrides and entrains Antarctic Bottom Water (AABW), of a largely Weddell Sea source[12], during its southward flow in the Atlantic. Assuming that the DOC concentrations reported here for the deep Circumpolar Current in the Pacific sector (170° W; Table 1) are the same as concentrations in AABW from the Weddell Sea (an assumption also made for the remaining discussion), then the mixing of these two source waters, microbial degradation, and other loss terms will result in a DOC

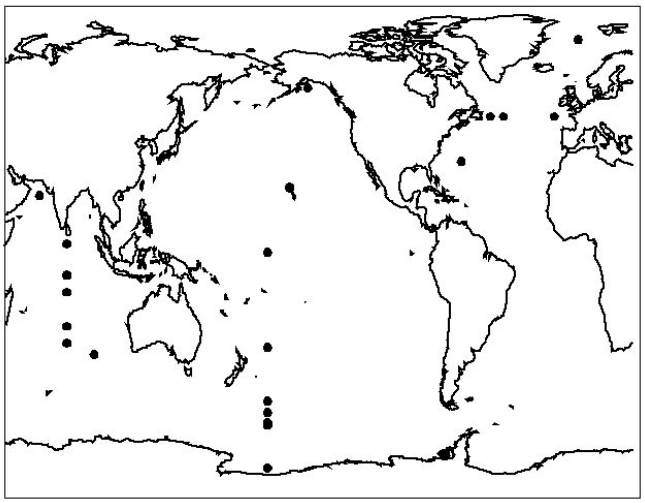

Figure 1 World map depicting locations sampled for the survey. Station locations are given in Table 1.

Table 2 Monthly variability in deep ocean DOC concentrations at two sites

Location	Period	DOC* (μM)	s.d.	*N*
Sargasso Sea	January	43.2	0.8	5
	February	43.5	0.2	7
	March	43.4	0.3	7
	April	43.4	–	2
	May	43.4	–	2
	June	43.6	0.5	7
	July	43.1	0.2	7
	August	43.5	0.7	6
	September	43.6	0.2	6
	October	43.4	0.3	7
	November	43.7	0.2	6
	December	43.7	0.2	6
Arabian Sea	July/August	42.5	0.8	97
	August/September	42.6	0.5	19
	November	42.9	0.8	85
	December	42.4	0.8	119

* Monthly variability in deep ocean DOC concentrations at two sites: the Sargasso Sea (32° N, 164° W; sampled in 1996) and the Arabian Sea (in the area bounded by 13–20° N, 60–65° E; sampled in 1995). The Sargasso Sea values result from the monthly visits made to the site of the US JGOFS Bermuda Atlantic time-series study. The analyses were done approximately every month. The mean values reported for the Arabian Sea are for all deep-water analyses performed during US JGOFS Arabian Sea Process Cruises 4, 5, 6 and 7, respectively. These cruises coincided with the hydrologically defined southwest Monsoon (July and August), autumn intermonsoon (November) and the northeast Monsoon (December). "Period" indicates the nominal month of sampling; *N*, number of depths sampled; s.d., standard deviation about the mean for the samples taken from *N* depths. Sampling depths ranged from 900 to >4,000 m. Arabian Sea Cruise 4 samples were analysed in the laboratory of E. Peltzer; all others were done in the Hansell laboratory. Note, there is low temporal variability relative to the gradients of deep ocean DOC shown in Table 1.

concentration gradient in the Atlantic Ocean, decreasing from north to south. Deep-water silicate concentrations in the Atlantic[13], useful for indicating the degree of mixing between the two components[12], suggest a dilution of NADW with ~10% AABW at the 32° N site. Such a dilution would account for a 0.6 μM decrease in DOC from Greenland Sea concentrations, so the remaining 3.8 μM decrease can be assigned to microbial consumption if it is the dominant loss term. The net rate of microbial utilization of DOC during the ~80-yr transit[7] from the site of NADW formation to the 32° N sampling site was 0.05 μM C yr^{-1}, or half the total organic carbon oxidation (sum of DOC and sinking biogenic carbon oxidation) estimated from apparent oxygen utilization rates in the deep central Atlantic[14]. Total DOC mineralization along the path of deep flow from the site of formation to 32° N is estimated at 0.64×10^{12} g C yr^{-1} (given 14 Sv (where 1 Sv = 10^6 m^3 s^{-1}) of NADW flow[15]).

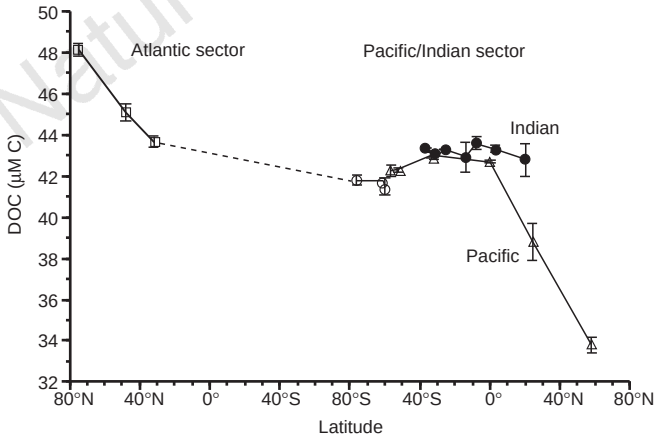

Figure 2 Mean concentrations of dissolved organic carbon (DOC; μM C) in the deep ocean. The means shown are of several depths at various sites in the global ocean (see Table 1 for locations and depth ranges sampled). The standard deviations of the means are shown as vertical bars through the data points. Solid lines connect data within ocean basins; the dashed line is used to demonstrate uncertainty in the South Atlantic Ocean as samples were not available for this analysis. Open boxes indicate data from the Atlantic Ocean, open circles the Southern Ocean, filled circles the Indian Ocean (including the Arabian Sea), and open triangles the Pacific Ocean.

Estimates of microbial utilization of DOC employing concentration gradients thought to develop over long distances and a multi-decadal period requires two primary assumptions: that concentrations of DOC reported here for the site of deep-water formation are constant, such that measurements made there now adequately reflect concentrations several decades earlier; and that neither deep winter convection in the Labrador Sea[16] nor diapycnal mixing of intermediate water of a Labrador Sea source alter deep DOC concentrations significantly. These assumptions are not testable with the current data set.

Deep water in the Indian and Pacific oceans have as their source AABW and NADW[17–19]. In the Indian Ocean, the Weddell Sea contributes to the densest water found in the western basins whereas the Ross Sea contributes to the eastern basins. The sampling conducted here (mostly along 80° E) was largely in the return flow of these source waters from the northern Indian Ocean. The raised concentration of DOC in the return flow may result from the introduction of DOC-rich subsurface water to the deep layers in the Arabian Sea and the Bay of Bengal. Outflow from marginal seas such as the Red Sea and the Persian Gulf could be particularly important. The subsurface Persian Gulf outflow (at 250 m in the mouth of the Gulf of Oman) has DOC concentrations in excess of 50 μM (ref. 20). It is likely that the Red Sea outflow, which reaches depths of 1,000 m in the Arabian Sea and has been reported as far south as 30° S (ref. 21), has similarly raised DOC concentrations. Alternatively, NADW may add DOC to the central Indian Ocean. NADW contributes 25 ± 10% of input to the deep Indian Ocean[12], so the increase in DOC observed along 80° E could be ascribed to NADW if concentrations in that water were ~48.5 μM as it entered the Indian Ocean. This requirement is unlikely to be met, given the decrease in DOC along the path of NADW flow from the North Atlantic shown in Fig. 2. If the northern Indian Ocean is the source of the new DOC, then an estimate of carbon export can be made. 15 Sv of return flow from the deep Indian Ocean to the circumpolar deep water[19], given the addition of 1.5 μM DOC, carries with it an additional carbon load of 8.5×10^{12} g DOC yr^{-1}.

Mechanisms for the DOC concentration increase seen from the deep Circumpolar Current north into the South Pacific are more difficult to identify, but entrainment of DOC-rich overlying waters may contribute. Geostrophic currents along the section sampled (170° W) are largely southward at depths of <3,000 m, and largely northward at depths >4,000 m (ref. 22). At intermediate depths, laterally adjacent currents flow in opposing directions. The south flowing waters are part of the subtropical gyre and equatorial upwelling systems, which have raised DOC concentrations above and in the main thermocline[23], whereas the northward flowing water is circumpolar deep water transiting the Samoan Passage into the deep equatorial and North Pacific region[24]. Shear between these current systems will enhance the exchange of constituents such as DOC, but exact mechanisms and locations of transfer are uncertain.

Deep water concentrations of DOC south (33.5° S) and north (Equator) of the Samoan Passage (near 10° S, 170° W) were very similar (Fig. 2), whereas the concentration decreased rather abruptly into the North Pacific. The deep North Pacific contains the world's oldest water relative to time since ventilation with the atmosphere[25], with inflow from the Samoan Passage as its principal source[19,24]. The very low DOC concentrations are likely to be due to microbial decomposition in excess of new carbon introduced by vertical entrainment or sinking particle solubilization. Additional loss of DOC in deep North Pacific waters has been proposed to occur by adsorption onto suspended particulate organic carbon[9], which could in turn fall from the water column. This process could take on particular significance over the timescales of deep ocean circulation.

The total organic carbon stock in the global ocean estimated from

the data in Table 1 and from ocean basin volumes is $\sim 685 \times 10^{15}$ g (57×10^{15} mol C), falling on the low side of existing estimates[3,5,26]. Given the size of the oceanic reservoir of organic carbon, the contribution of this pool to the global carbon cycle remains surprisingly poorly resolved. With the clear signals for DOC concentration gradients in the deep ocean, large transformations and transport of organic carbon are evident. Concentration differences between the North Atlantic and the North Pacific result from differences in the thermohaline circulation patterns in those basins. The deep North Atlantic Ocean is filled with water relatively recently at the surface, with strong contributions of DOC-enriched subtropical gyre water via the North Atlantic Current. The deep North Pacific, on the other hand, is flushed by circumpolar deep water of an Antarctic source, with quite low initial concentrations of DOC (Fig. 2).

Further speculation on the biological and physical processes forcing the deep-ocean DOC signals will require a much larger and spatially complete survey of deep and intermediate ocean DOC concentrations. Regions of focus must include the Arctic Ocean (where increased DOC concentrations have been reported[27]), the Weddell Sea (primary site of AABW formation), and the major sites of mode and intermediate water formation. We have assumed throughout this discussion that deep Weddell Sea water has DOC concentrations very similar to those of the measured Circumpolar and Ross Sea waters in the Pacific sector. Such may be a reasonable assumption, given the uniform distribution of other variables, such as $\Delta^{14}C\text{-}CO_2$, in the circumpolar waters[25]. Higher concentrations of organic carbon have been reported, however, in the deep Weddell Sea[28], but comparison between data sets is not possible because a common analytical reference material was not used. These uncertainties highlight the need for a broadened and fully referenced survey of the deep ocean in order to identify the role of marine DOC in the oceanic carbon cycle. □

Received 26 January; accepted 30 June 1998.

1. Hedges, J. I. Global biogeochemical cycles: progress and problems. *Mar. Chem.* **39,** 67–93 (1992).
2. Menzel, D. W. The role of *in situ* decomposition of organic matter on the concentrations of non-conservative properties in the sea. *Deep-Sea Res.* **17,** 751–764 (1970).
3. Martin, J. H. & Fitzwater, S. E. Dissolved organic carbon in the Atlantic, Southern and Pacific Oceans. *Nature* **356,** 699–700 (1992).
4. Barber, R. T. Dissolved organic carbon from deep waters resist microbial oxidation. *Nature* **220,** 274–275 (1968).
5. Williams, P. M. & Druffel, E. R. M. Radiocarbon in dissolved organic matter in the central North Pacific Ocean. *Nature* **330,** 246–248 (1987).
6. Bauer, J. E., Williams, P. M. & Druffel, E. R. M. ^{14}C activity of dissolved organic carbon fractions in north-central Pacific and Sargasso Sea. *Nature* **357,** 667–670 (1992).
7. Broecker, W. S. The great ocean conveyor. *Oceanography* **4,** 79–89 (1991).
8. Smith, D., Simon, M., Alldredge, A. L. & Azam, F. Intense hydrolytic enzyme activity on marine aggregates and implications for rapid particle dissolution. *Nature* **359,** 139–142 (1992).
9. Druffel, E. R. M., Bauer, J. E., Williams, P. M., Griffin, S. & Wolgast, D. Seasonal variability of particulate organic radiocarbon in the northeast Pacific Ocean. *J. Geophys. Res.* **101,** 20543–20552 (1996).
10. Deuser, W. G. in *Scope 57 Particle Flux in the Ocean* (eds Ittekkot, V., Schafer, P., Honjo, S. & Depetris, P. J.) 185–198 (Wiley, New York, 1996).
11. Honjo, S., Dymond, J., Prell, W. & Manganini, S. J. Monsoon controlled export fluxes to the interior of the Arabian Sea: JGOFS 1994–95 Experiment. *Deep-Sea Res. II* (submitted).
12. Broecker, W. S. & Peng, T.-H. *Tracers in the Sea* (Lamont Doherty Geological Observatory, Columbia University, Palisades, NY, 1982).
13. Knap, A. H. *et al. BATS Data Report B-5* (US JGOFS Planning and Coordination Office, Woods Hole Oceanographic Institution, MA, 1995).
14. Broecker, W. S., Blanton, S., Smethie, W. M. & Ostlund, G. Radiocarbon decay and oxygen utilization in the deep Atlantic Ocean. *Global Biogeochem. Cyc.* **5,** 87–117 (1991).
15. Schmitz, W. J. Jr *On the World Ocean Circulation, I* (Woods Hole Oceanographic Institution Technical Report WHOI-96-03, MA, 1996).
16. Sy, A. *et al.* Surprisingly rapid spreading of newly formed intermediate waters across the North Atlantic Ocean. *Nature* **386,** 675–679 (1997).
17. Reid, J. L. & Lynn, R. J. On the influence of the Norwegian–Greenland and Weddell seas upon the bottom waters of the Indian and Pacific oceans. *Deep-Sea Res.* **18,** 1063–1088 (1971).
18. Mantyla, A. W. & Reid, J. L. On the origins of deep and bottom waters of the Indian Ocean. *J. Geophys. Res.* **100,** 2417–2439 (1995).
19. Schmitz, W. J. Jr *On the World Ocean Circulation, I* (Woods Hole Oceanographic Institution Technical Report WHOI-96-08, MA, 1996).
20. Hansell, D. A. & Peltzer, E. T. Spatial and temporal variations of total organic carbon in the Arabian Sea. *Deep-Sea Res. II* (in the press).
21. Dileep, K. M. & Li, Y.-H. Spreading of water masses and regeneration of silica and ^{226}Ra in the Indian Ocean. *Deep-Sea Res. II* **43,** 83–110 (1996).
22. Reid, J. L. On the total geostrophic circulation of the South Pacific Ocean: Flow patterns, tracers and transports. *Prog. Oceanogr.* **16,** 1–61 (1986).
23. Hansell, D. A. & Waterhouse, T. Y. Controls on the distribution of organic carbon and nitrogen in the eastern Pacific Ocean. *Deep-Sea Res. I* **44,** 843–857 (1997).
24. Roemmich, D., Hautala, S. & Rudnick, D. Northward abysall transport through the Samoan passage and adjacent regions. *J. Geophys. Res.* **101,** 14039–14055 (1996).
25. Stuiver, M., Quay, P. D. & Ostlund, H. G. Abyssal water carbon-14 distribution and the age of the world oceans. *Science* **219,** 849–851 (1983).
26. Druffel, E. R. M., Williams, P. M., Bauer, J. E. & Ertel, J. R. Cycling of dissolved and particulate organic matter in the open ocean. *J. Geophys. Res.* **97,** 15630–15659 (1992).
27. Anderson, L. G., Olsson, K. & Skoog, A. in *The Polar Oceans and Their Role in Shaping the Global Environment* (eds Johannessen, O. M., Muench, R. D. & Overland, J. E.) 255–262 (Geophys. Monogr. Ser., Am. Geophys. Union, Washington DC, 1994).
28. Wedborg, M., Hoppema, M. & Skoog, A. On the relation between organic and inorganic carbon in the Weddell Sea. *J. Mar. Syst.* (in the press).
29. Hansell, D. A., Carlson, C. A., Bates, N. & Poisson, A. A re-assessment of carbon export in the Equatorial Pacific Ocean. *Deep-Sea Res. II* **44,** 2115–2130 (1997).

Acknowledgements. We thank R. Parsons for her fine analytical work and T. Weingartner, D. Karl, D. Wallace and J. Urban-Rich for assistance during sample collections. This work was supported by the US NOAA and NSF.

Correspondence and requests for materials to D.A.H. (e-mail: dennis@bbsr.edu).

Plastic deformation of silicate spinel under the transition-zone conditions of the Earth's mantle

Shun-ichiro Karato*, Catherine Dupas-Bruzek† & David C. Rubie†

** University of Minnesota, Department of Geology and Geophysics, Minneapolis, Minnesota 55455, USA*

† Bayerisches Geoinstitut, Universität Bayreuth, D-95440, Germany

The dynamics of the Earth's deep interior are controlled to a large extent by rheological properties[1,2]. Until recently, however, experimental studies on the rheological properties of materials thought to be present in the Earth's deep interior have been limited to relatively low pressures. Most previous estimates of rheology have therefore been based on either large extrapolations of low-pressure experimental data[3,4] or inferences from geodynamical observations[5–7]. Such studies have provided only weak constraints on the complicated rheological structure expected in the transition zone of the Earth's mantle (between 410 and 660 km depth) where a series of phase transformations occur in silicate minerals[8]. Here we report the results of a direct experimental study of deformation, under transition-zone conditions, of the spinel phase of $(Mg,Fe)_2SiO_4$ (ringwoodite; thought to be present in the Earth's transition zone). Relatively coarse-grained samples show evidence of dislocation creep with dislocation structures similar to those observed in oxide and germanate spinels[9,10], which have significantly higher creep strengths than olivine[10,11]. In contrast, a fine-grained sample shows evidence for grain-size-sensitive creep. These observations suggest that a ringwoodite-rich layer of the transition zone is likely to have a higher viscosity than the olivine-rich upper mantle[3], whereas a subducting slab in the deep transition zone may lose its strength if significant grain-size reduction occurs[12–14].

Recent high-resolution seismic tomography[15–17] and numerical modelling[18–21] suggest that the interactions of convection currents

Table 1 Summary of experiments

Run	P (GPa)	T (K)	t (h)	d (μm)	γ (%)
no. 704	16	1,400	5	0.4 (S)* 3 (L)†	56
no. 710	16	1,600	5	6	‡
no. 1740	16	1,600	10	5	102

Here P is pressure, T is temperature, t is time, d is grain-size, and γ is shear strain.
* Most of the sample. S indicates small grains.
† A few grains occupying <0.1% of the sample volume. L indicates large grains.
‡ Strain was not measured because the sample was cut at a wrong orientation.